Novel Dual-Phase-Shift Control With Bidirectional Inner Phase Shifts for a Dual-Active-Bridge Converter Having Low Surge Current and Stable Power Control

X. Liu, *Senior Member, IEEE*, Z. Q. Zhu, *Fellow, IEEE*, David A. Stone, Martin P. Foster, W. Q. Chu, Iain Urquhart, and James Greenough

***Abstract*—To transmit constant powers particularly at light load, the isolated dual active bridge (DAB) with conventional dual-phase-shift (DPS) control exhibits large variations of currents, losses, and efficiencies if there is a small change of outer phase shift ratio, which is caused by the change of command to adjust power transmission. This is mainly because of the narrow operation region of outer phase shift ratio if the conventional DPS modulation is used. To solve this problem, a novel DPS control with bidirectional inner phase shifts for the DAB is developed to reduce the current surge in the high-frequency transformer, which can stabilize the output power with high efficiency. From the analysis of operation modes and power characteristics of the proposed DPS control, it is shown that due to wider operation region of outer phase shift ratios compared with the conventional DPS control in which the inner phase shifts of both the primary and secondary H-bridges are in the same direction, lower surge current can be obtained in the change of phase shift command, which results in stable power transmission particularly at light load without scarifying the efficiency. Moreover, the DAB of using the proposed DPS control can transmit bidirectional energy with the inner and outer shift ratios of 0–1. For experimental verifications, the test results are also presented in this paper.**

***Index Terms*—Bidirectional inner phase shifts, dual-active-bridge (DAB) dc–dc converter, dual-phase-shift (DPS) modulation, efficiency.**

I. Introduction

DUE to the concern of environment, electric vehicles (EVs) and hybrid electric vehicles (HEVs) have obtained more and more attentions. However, a fast and safe charger as an interface between the grid and vehicles or renewable energy and vehicles is crucial to the success of EVs and HEVs. Due to the galvanic isolation, bidirectional power flow, and high efficiency, dual-active-bridge (DAB) dc–dc converters have been considered to be promising for the automotive applications [1]–[8].

To control the energy flow between the primary and secondary H-bridges in the DAB, the most convenient approach is the single-phase-shift (SPS) control due to its simplicity and zero-voltage switching (ZVS) if the ratio of primary and secondary voltages equals the transformer turn ratio [8]–[10]. However, since the shift angle of the secondary phase voltage respective to the primary phase voltage is the only parameter to manipulate the transmission active power, the reactive power, which requires larger filter, increases copper loss, and reduces the efficiency, is not controllable in the conventional SPS control. In [16]–[18], the trapezoidal modulation and the triangular modulation were developed to operate the DAB with different ratio of primary and secondary voltages from the transformer ratio. Since one or two switch legs are changed from ZVS to zero-current switch (ZCS) in these modulations, higher efficiency can be obtained. In addition, pulse width modulation (PWM) together with SPS was proposed to extend the ZVS region to light load [11]–[15]. PWM controls of one H-bridge or two H-bridges were analyzed to operate the DAB [11]. The soft-switching ranges are investigated in the DAB with single-H-bridge PWM or dual-H-bridge PWM. It shows the efficiency benefit of the DAB at light load if dual-H-bridge PWM is employed, since the soft-switching range can obtained at light load. However, the PWM duty cycles are restricted by the primary and secondary voltages and shift angle. The existing of freewheel intervals can result in the control failure of the DAB with PWM and phase shift control. Thus, a complicate control algorithm is required to avoid the failure mode of the DAB. In [13] and [14], the duty cycle and shift angle in the DAB with single-H-bridge PWM are optimized to reduce the losses and maximize the system efficiency. It can be treated as a special case of the DAB with dual-H-bridge PWM, and risk of failure mode also exists. Moreover, the reactive power, i.e., circulating energy, can still be observed in PWM control of the DAB. In [19]–[23], a dual-phase-shift (DPS) control was developed and analyzed with the advantage of zero reactive power in the DAB so as to produce higher efficiency.

Manuscript received February 14, 2016; revised May 14, 2016; accepted July 4, 2016. Date of publication July 22, 2016; date of current version February 2, 2017. Recommended for publication by Associate Editor D. Xu.

X. Liu was with the Department of Electronic and Electrical Engineering, The University of Sheffield, Sheffield, S1 3JD, U.K. He is now with Hebei University of Technology, Tianjin 300130, China (e-mail: liuxuee@gmail.com).

Z. Q. Zhu, D. A. Stone, M. P. Foster, and W. Q. Chu are with the Department of Electronic and Electrical Engineering, The University of Sheffield, Sheffield S1 3JD U.K (e-mail: z.q.zhu@sheffield.ac.uk; d.a.stone@sheffield.ac.uk; m.p.foster@sheffield.ac.uk; chu.wenqiang@gmail.com).

I. Urquhart and J. Greenough are with Nissan Motor Manufacturing Ltd., Sunderland SR5 3NS U.K (e-mail: Iainurqhrt@gmail.com; Jim.Greenough@ntc-europe.co.uk).

Color versions of one or more of the figures in this paper are available online at http://ieeexplore.ieee.org.

Digital Object Identifier 10.1109/TPEL.2016.2593939

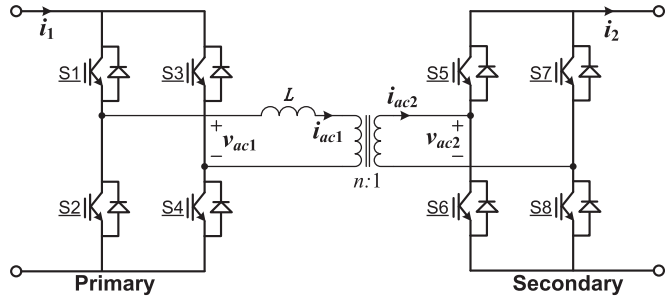

Fig. 1. Schematic of the DAB.

Compared with the conventional SPS control, there are two independent parameters to manipulate the energy flow in the DAB with the DPS control. In [20], it is reported that unity power factor and high efficiency can be obtained by carefully choosing the combination of the inner and outer phase shift ratios. However, the DPS control requires the sum of inner and outer phase shift ratios, D_1 and D_2, equal to or less than 1, i.e., $D_1+D_2\leq 1$. This is because if the sum of D_1 and D_2 is higher than 1, the outer phase shift ratio will not be able to control the power flow. Moreover, in the conventional DPS control, it is found that at light load, a large variation of inner phase shift D_1 will be observed if the command of power transmission is changed, as will be illustrated in Section II. This disadvantage may result in larger surge current during the transient and reduce the stabilization of power transmission particularly at light load. To solve this problem, a novel DPS control with bidirectional inner phase shifts is developed to extend the operation regions of inner and outer phase shift ratios. Compared with the single and dual PWM H-bridge DAB presented in [11], [14], the duty cycles of all switches in the proposed DPS will be fixed. Thus, the freewheel intervals, which require complicate control algorithm to avoid, can be eliminated in the proposed DPS. By using the proposed DPS control, the surge current is significantly reduced, while the stabilization of power transmission is improved without scarifying the efficiency. This paper will be organized as follows. In Section II, the merits and drawbacks of conventional SPS and DPS controls will be presented. Section III will present the principle and operation mode analysis of the novel DPS control with bidirectional inner phase shifts. In Section III, the principle of novel DPS with bidirectional inner phase shifts will be presented together with its performance. Experimental verifications of the novel DPS control and the comparison of the conventional DPS control will be presented in Sections IV and V, respectively.

II. Conventional Phase Shift Control and DPS Control

A. SPS Control

Fig. 1 shows the schematic of an isolated DAB dc–dc converter. Inductance L is the leakage inductance of a high-frequency transformer. In the SPS control, all switches are operated with 50% duty cycle. The power flow is controlled by the shift angle φ, as illustrated in Fig. 2. The positive shift angle is defined as the primary voltage leading the secondary voltage, since the energy flows from the primary side to the secondary side. By neglecting the losses, the transmission power can be expressed by (1), where V_1, V_2, L, and f_s are the primary and secondary voltages, leakage inductance, and switching frequency, respectively

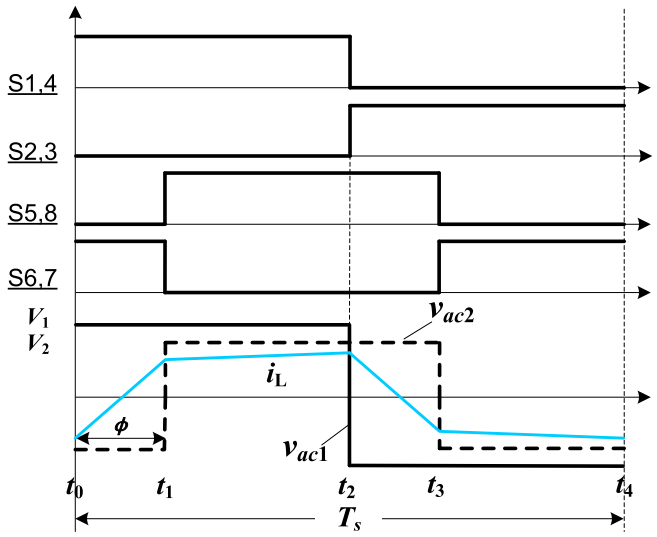

Fig. 2. Drive signal and corresponding current and voltage waveforms in the DAB with the SPS control.

$$P=\frac{nV_1V_2(\pi-|\varphi|)\varphi}{2\pi^2Lf_s}. \tag{1}$$

From Fig. 2, larger circulating current can be observed during the power transmission, which is also known as reactive power [19]. To reduce or even eliminate the reactive power, the DPS control was developed, as will be illustrated in the next part.

B. Conventional DPS Control

Fig. 3 illustrates the conventional DPS control and its corresponding current and voltage waveforms. Compared with the SPS control, the power flow is controlled not only by the phase shift between the primary and secondary voltages (outer phase shift) but also the phase shift between the legs in the primary and the secondary H-bridges (inner phase shift). By neglecting the losses of the DAB, the power flow under the DPS control can be expressed as

$$P=\begin{cases}-\frac{nV_1V_2(D_1^2+2(-1+D_2)D_2)}{4Lf_s}, & D_1<D_2\\ -\frac{nV_1V_2D_2(-2+2D_1+D_2)}{4Lf_s}, & D_1\geq D_2\end{cases} \tag{2}$$

where D_1 and D_2 are inner and outer phase shift ratios. The inner phase shift is defined as the phase shift between the legs in the H-bridge, and the outer phase shift is defined as the phase between the primary and secondary sides. $T_{\rm hs}$ in Fig. 3 stands for the period of switching. $D_1T_{\rm hs}$ and $D_2T_{\rm hs}$ are the inner and outer phase shift angles. However, to employ the DPS control, the inner and outer phase shift ratios are required to satisfy (3), since the power flow will not be controlled by D_2 if the sum of D_1 and D_2 is higher than 1, as can be noticed from Fig. 3

$$D_1+D_2\leq 1. \tag{3}$$

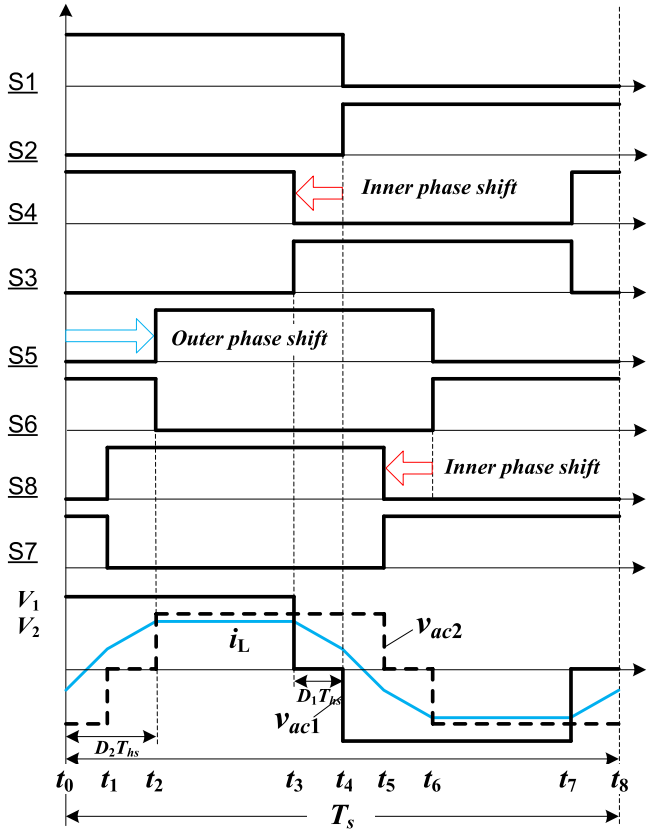

Fig. 3. Drive signals and corresponding current and voltage waveforms in the DAB with the DPS control.

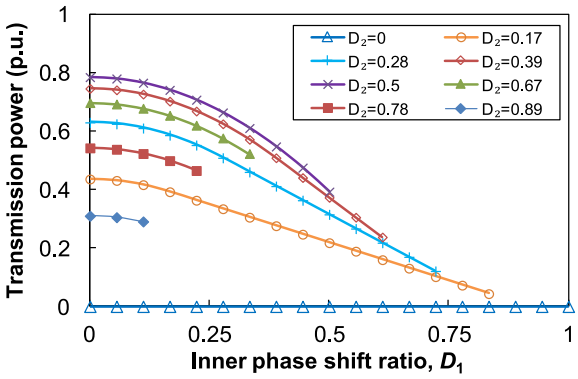

Fig. 4. Transmission power against inner and outer phase shift ratios.

By defining the base value of transmission power

$$P_B = \frac{nV_1V_2}{2\pi Lf_s} \tag{4}$$

the transmission power per unit against inner phase shift ratio at different outer phase shift ratios can be obtained in Fig. 4. As D_2 increases, the operation region of D_1 will be significantly reduced. It is shown that as D_2 increases, the operation range of D_1 will be significantly reduced. For example, when D_2 equals 0.89, the operation range of D_1 should be less than

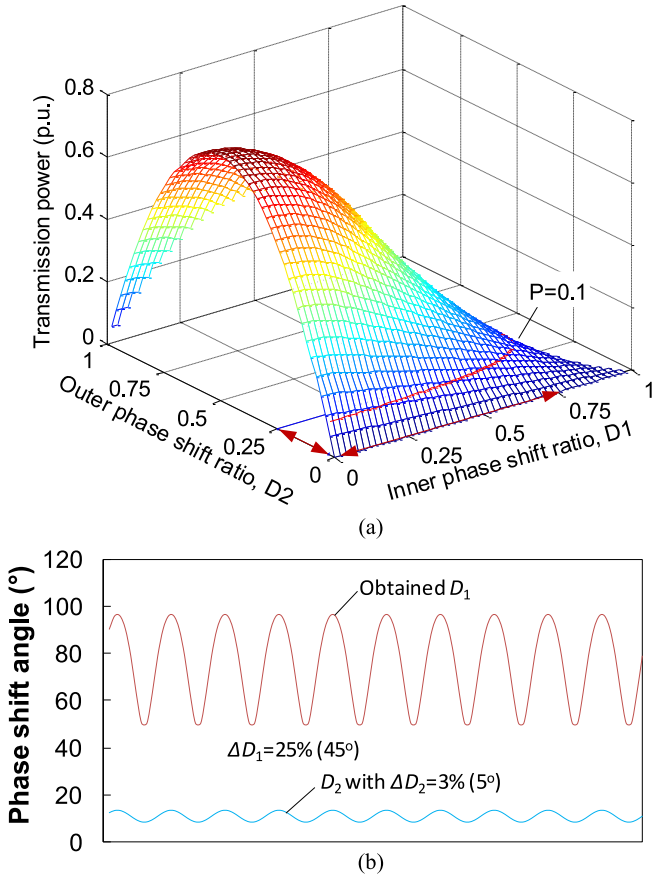

Fig. 5. Illustration of inner and outer phase shift regions for particular power transmission.

0.1. The operation of D_1 higher than 0.1 will lead to the DAB out of control. Moreover, for a constant power flow, infinite combinations of D_1 and D_2 can be used. In [22], a control strategy for constant power flow is to calculate the D_1 from the transmission power command and predefined D_2, which can be used to control the output voltage. Then, the inner phase shift ratio D_1 will be calculated by

$$D_1 = \begin{cases} \sqrt{2D_2 - 2D_2^2 - \frac{P}{k}}, & D_1 < D_2 \\ 1 - \frac{D_2}{2} - \frac{P}{2D_2 k}, & D_1 \geq D_2 \end{cases} \tag{5}$$

where

$$k = \frac{nV_1V_2}{4Lf_s}. \tag{6}$$

Fig. 5(a) shows the power characteristic of the DAB with the conventional DPS control. With D_1 and D_2 in operation region of 0–1, the energy flows from the primary to the secondary side. The power flow can be reversed if the outer phase shift ratio D_2 is less than zero. With the aid of (5), the feasible D_1 and D_2 combinations with a constant power transmission are illustrated in Fig. 5(a). Taking the transmission power, $P = 0.1$ (p.u.) for example, the feasible D_1 and D_2 regions are 0–0.75 and 0–0.25, respectively. Fig. 5(b) shows that the calculated D_1 is

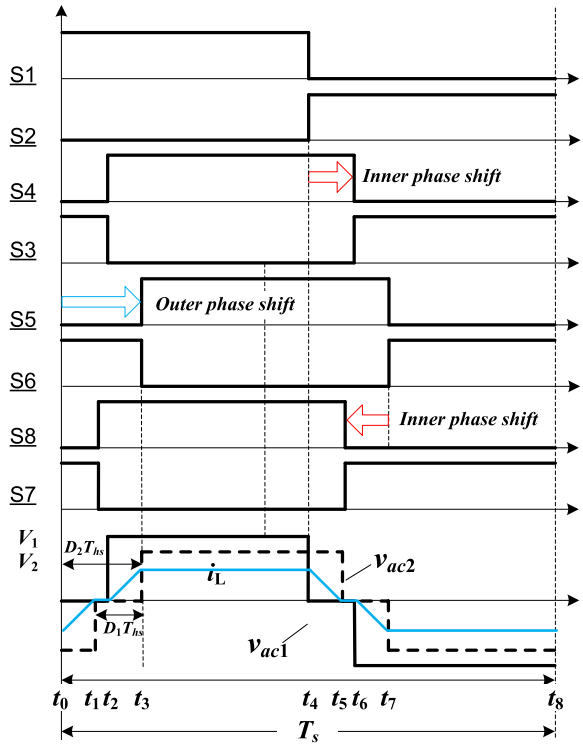

Fig. 6. DPS control with bidirectional inner phase shifts.

very sensitive to D_2, i.e., a small ΔD_2 will result in significant variation of D_1, which will result in significant variation of current and further lead to significant variations of switching loss and efficiency particularly at light load, as will also be illustrated by the tests in Section V. In order to solve this problem, a modified DPS modulation is proposed, as will be introduced in the next section.

In addition, since the digital microprocessors have been widely used to control the DAB, the calculation error due to the limited length of data byte can also lead to inaccurate power transmission [24].

III. Proposed DPS Control With Bidirectional Inner Phase Shifts

A. Basic Principle

From the previous analysis, it is shown that since the feasible region of D_2 is much less than that of D_1 particularly at light load, significant variation of D_1 due to a small ΔD_2 will not be avoidable. In order to enlarge the operation region of D_2, a modified DPS control with bidirectional inner phase shifts is proposed, as illustrated in Fig. 6. Although all switches are operated with a fixed 50% duty cycle, the voltage and current waveforms in both the primary and secondary sides can be controlled, similar to the PWM-controlled SPS modulation. Different from the conventional DPS control, in which the inner phase shifts of both the primary and secondary H-bridges are in the same direction, in the proposed DPS control, the inner phase shifts of the primary and secondary H-bridges are in bidirectional directions. Thus, the conventional DPS can be treated as a special case of the proposed DPS. However, this paper will focus on the operation case of the DPS control, with the inner phase shifts of the primary and secondary H-bridges are in opposite directions. The conventional scheme can transit seamless to the proposed strategy by setting the inner phase ratio D_1 to zero without stopping the power transmission. This modification will lead to the change of operation regions of inner and outer phase shift angles. The operation regions of inner and outer phase shift angles can be enlarged particularly at light load, as will be illustrated in the next section. The definition of inner and outer phase shifts D_1 and D_2 in the modified DPS is the same as that in the conventional DPS, i.e., the phase shift between the H-bridge legs is defined as the inner phase shift D_1, and the phase shift between the primary and secondary sides is defined as the outer phase shift D_2, as shown in Fig. 6.

B. Operation Modes

As shown in Fig. 6, the DPS control with bidirectional inner phase shifts can be operated in three cases, i.e., $0 < D_1 \leq D_2/2$, $D_2/2 < D_1 \leq D_2$, $D_2 < D_1 \leq (D_2+1)/2$. The limitation for D_1 and D_2 is $2D_1 - D_2 \leq 1$. Compared with the limitation of D_1 and D_2 with the conventional DPS, larger operation region can be obtained in the novel DPS control. The operation modes is illustrated by taking one case, i.e., $D_2/2 < D_1 \leq D_2$ together with $V_1 = nV_2$, for example.

1) *Mode 1* ($t_0 - t_1$): As shown in Fig. 7(a), at t_0, S2 is turned OFF. Due to the negative current i_L, the current will flow through S3 and D1. Therefore, S1 will be turned ON at ZVS. On the secondary side, the current will flow through D6 and D7 and the voltage across L is nV_2. This mode will end up with switching on of S8. During this mode, the current through L can be expressed as

$$i(t) = i(t_0) + \frac{nV_2}{L}(t - t_0). \tag{7}$$

2) *Mode 2* ($t_1 - t_2$): At t_1, since the primary voltage V_1 equals nV_2, S7 is turned OFF and S8 is turned ON at ZCS. However, if nV_2 is higher than V_1, S8 will be turned ON at ZVS and S7 has hard switching OFF [see Fig. 7(b)]. If nV_2 is lower than V_1, S7 is turned OFF at ZVS and S8 has hard switching ON. During this mode, the voltage across L is zero. This mode will be end up with switching on of S4. The current of L in this mode is kept the same, i.e.,

$$i(t) = i(t_1). \tag{8}$$

3) *Mode 3* ($t_2 - t_3$): This mode will start with switching OFF of S3. S4 is turned ON at ZCS if $V_1 = nV_2$. However, if nV_2 is higher than V_1, S3 will be turned OFF at ZVS and S4 has hard switching ON [see Fig. 7(c)]. If nV_2 is lower than V_1, S4 is turned ON at ZVS and S3 has hard switching OFF. During this mode, the current of L flows through S1, S4, S6, and D8. This mode will end up with switching OFF of S6. The current of L can be

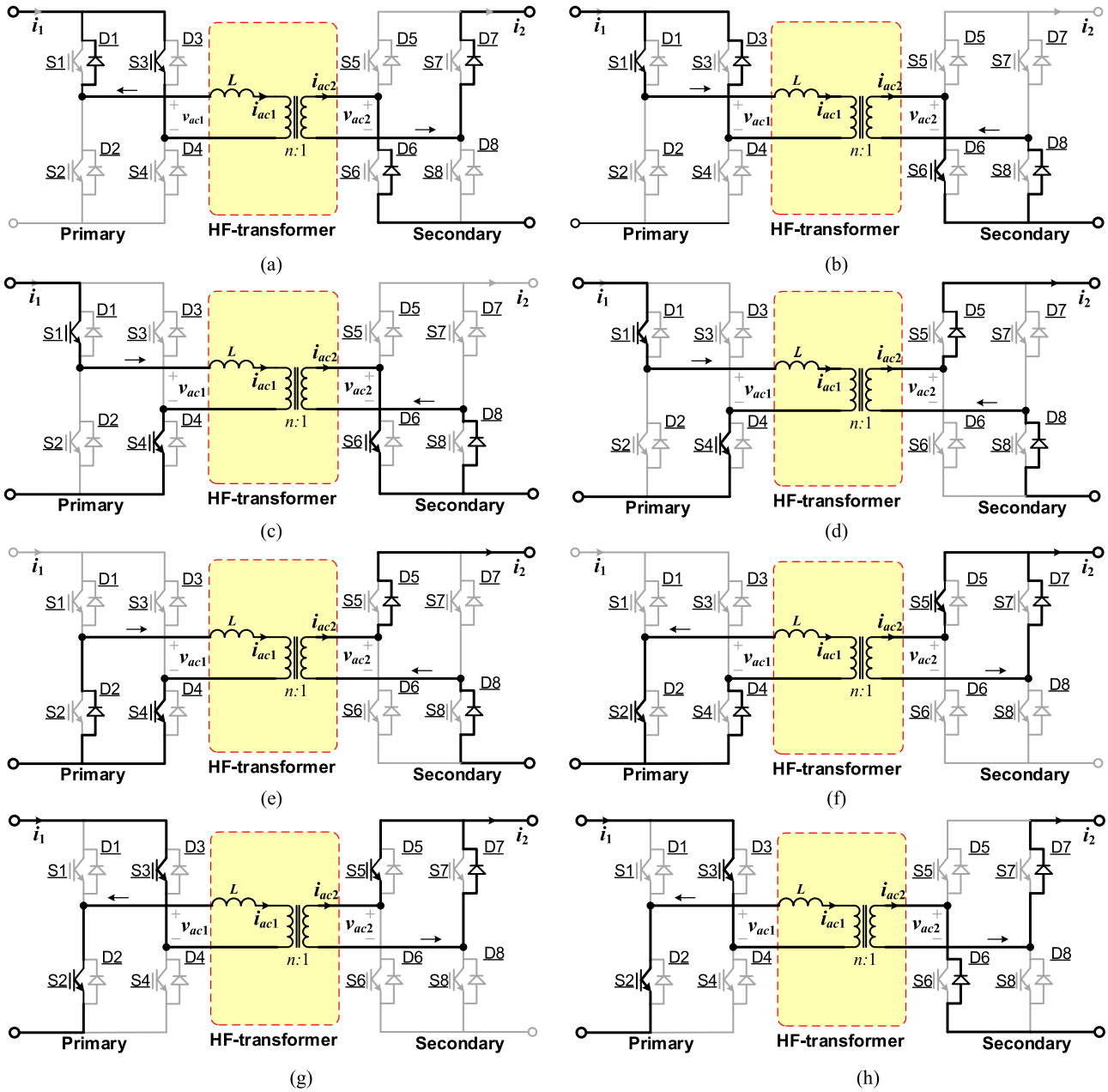

Fig. 7. Operation modes of the DAB using the DPS control with bidirectional inner phase shifts.

calculated by

$$i(t) = i(t_2) + \frac{V_1}{L}(t - t_2). \tag{9}$$

4) *Mode 4* ($t_3 - t_4$): At t_3, S6 is turned OFF. Due to the positive current, the current will flow through D5 and D8, as shown in Fig. 7(d). S5 is turned ON at ZVS. The current in the primary side will flow through S1 and S4. During this mode, the voltage across L is $V_1 - nV_2$, and the current through L is

$$i(t) = i(t_3) + \frac{V_1 - nV_2}{L}(t - t_3). \tag{10}$$

5) *Mode 5* ($t_4 - t_5$): This mode starts from switching OFF of S1. Due to the positive current, the current i_L will flow through D2 and S4, as shown in Fig. 7(e). S2 can be turned ON at ZVS. This mode will be end up with switching ON of S7. During this mode, the current i_L can be expressed by

$$i(t) = i(t_4) - \frac{nV_2}{L}(t - t_4). \tag{11}$$

6) *Mode 6* ($t_5 - t_6$): At t_5, S8 is turned OFF and S7 is turned ON at ZCS if $V_1 = nV_2$ [see Fig. 7(f)]. However, if nV_2 is higher than V_1, S8 will have hard switching OFF, and S7 is turned ON at ZVS, while, if nV_2 is lower than V_1, S8 is turned OFF at ZVS and S7 has hard switching ON.

Since the voltage across L is zero, the current through L will be

$$i(t) = i(t_5). \tag{12}$$

7) *Mode 7* $(t_6 - t_7)$: In this mode, S4 is turned OFF and S3 is turned ON at ZCS if $V_1 = nV_2$ [see Fig. 7(g)]. However, if nV_2 is higher than V_1, S4 is turned OFF at ZVS and S3 has hard switching ON. While if nV_2 is lower than V_1, S3 is turned ON at ZVS and S4 has hard switching OFF. Since the voltage across the L is clamped to V_1, the current through L can be calculated as

$$i(t) = i(t_6) - \frac{V_1}{L}(t - t_6). \tag{13}$$

8) *Mode 8* $(t_7 - t_8)$: At t_7, S5 is turned OFF. Due to the negative current through L, the current will flow through D6 and D7. Thus, S6 is turned ON at ZVS. During this mode, the current of L can be calculated as

$$i(t) = i(t_7) - \frac{V_1 - nV_2}{L}(t - t_7). \tag{14}$$

In one switching cycle, due to

$$i(t) = i(t_1) \tag{15}$$

the initial current of L can be obtained by solving (15), i.e.,

$$i(t_0) = \frac{((-1 + D_1)V_1 + (1 + D_1 - 2D_2)nV_2)}{4Lf_s}. \tag{16}$$

C. Transmission Power

Based on the analysis of operation modes, the transmission power of the DAB with the novel DPS control can be obtained. By neglecting the losses, the transmission power can be expressed as follows:

Case I: $0 < D_1 \leq D_2/2$,

$$P = -\frac{nV_1V_2(3D_1^2 + D_1(2 - 4D_2) + 2D_2(D_2 - 1))}{4Lf_s}. \tag{17}$$

Case II: $D_2/2 < D_1 \leq D_2$,

$$P = \frac{nV_1V_2(-2D_1 + D_1^2 - (-2 + D_2)D_2)}{4Lf_s}. \tag{18}$$

Case III: $D_2 < D_1 \leq (D_2 + 1)/2$,

$$P = \frac{nV_1V_2(3D_1^2 + D_2(D_2 + 2) - 2D_1(1 + 2D_2))}{4Lf_s}. \tag{19}$$

Fig. 8 shows the transmission power against D_1 at different outer phase shift ratios. Compared with the conventional DPS control, the operation regions of D_1 and D_2 have been enlarged. Regardless of D_2 and D_1, the feasible operation region of 0–0.5 can be used to manipulate the DAB. In addition, with the operation region of 0–1, bidirectional power flow can be obtained by using the DPS control without setting D_2 to negative, which is used to change the direction of power flow in the conventional DPS. If $D_1 < D_2$, positive power flow can be obtained, while if $D_1 > D_2$, the energy can flow in the opposite direction. Zero power transmission is obtained if D_1 equals D_2. However, the maximum values of power flow in two directions

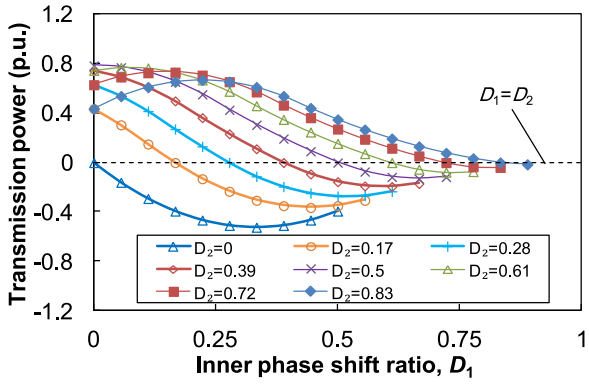

Fig. 8. Transmission power against inner and outer phase shift ratios.

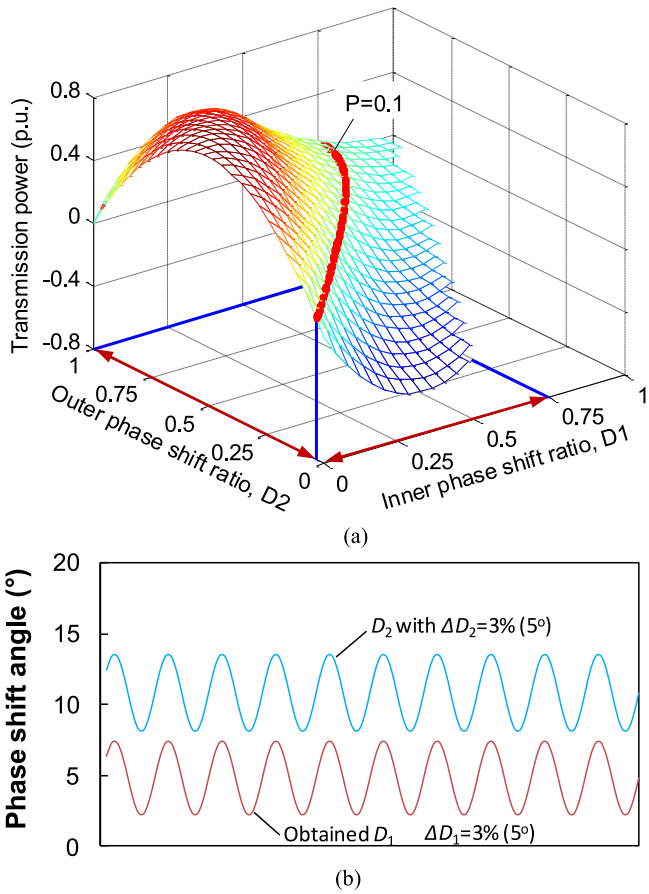

Fig. 9. Illustration of inner and outer phase shift regions for particular power transmission using the DPS control with bidirectional inner phase shifts.

are different. Higher power flow can be obtained in the direction of primary to the secondary side.

Similar to the conventional DPS control, to transmit constant power, infinite combinations of D_1 and D_2 can be used if the DPS control with bidirectional inner phase shifts is used [see Fig. 9(a)]. It is shown that with the operation region of D_1 and D_2, a bidirectional power flow can be realized by using the proposed method. To control the transmission power, the D_1 and D_2 combination is determined by a predefined D_2 and

calculated D_1. The D_2 can be obtained from a lookup table determined by the command power, while D_1 can be calculated from (20)–(22) according to D_2 and the command power. The direction of power flow can be precisely controlled by D_2 and D_1, which is calculated from D_2 and the command power.

Fig. 9 shows the power characteristic of using the DPS control with bidirectional inner phase shifts. Taking the transmission power of 0.1 (p.u.) for example, the feasible regions of D_1 and D_2 have been extended to 0–0.75 and 0–1, respectively. Compared with conventional DPS modulation, the feasible region of D_2 has been enlarged from 0–0.25 to 0–1, while a similar feasible region of D_1 can be observed. Fig. 9(b) shows that a small change of D_2, $\Delta D_2 = 3\%$ will not result in a significant variation of D_1. Thus, more stable current waveforms can be obtained.

Case I: $0 < D_1 \le D_2/2$

$$D_1 = -\frac{1}{3} + \frac{2}{3}D_2 \pm \frac{1}{3}\sqrt{1 + 2D_2 - 2D_2^2 - 3\frac{P}{k}}. \quad (20)$$

Case II: $D_2/2 < D_1 \le D_2$

$$D_1 = 1 \pm \sqrt{1 - 2D_2 + D_2^2 + \frac{P}{k}}. \quad (21)$$

Case III: $D_2 < D_1 \le (D_2 + 1)/2$

$$D_1 = \frac{1}{3} + \frac{2}{3}D_2 \pm \frac{1}{3}\sqrt{1 - 2D_2 + D_2^2 + 3\frac{P}{k}}. \quad (22)$$

The reactive power by using the DPS control with bidirectional inner phase shifts is similar to that of using conventional DPS modulation. The currents and voltages in the primary and secondary sides are alternating with positive and negative values. The sign of primary current is not always the same as the primary voltage. Thus, the energy with different signs of primary current and voltage will flow back to the source and is defined as reactive power. The reactive power of using the DPS control with bidirectional inner phase shifts can be expressed by (23) if $0 < D_1 \le D_2/2$. However, if $D_2/2 < D_1 \le (D_2 + 1)/2$, i.e., Cases II and III, the reactive power will be zero, which is the advantage of conventional DPS. From the investigation of reactive power, it can also be noticed that in the proposed method, the advantage of zero reactive power can also be obtained

$$Q = -\frac{V_1((-1 + D_1)V_1 + (1 + 3D_1 - 2D_2)nV_2)^2}{32Lf_s(V_1 + nV_2)}. \quad (23)$$

D. Switching-State Analysis

The switching states in the DAB of using the DPS control with bidirectional inner phase shifts can be obtained by the analysis of operation modes. However, since under different conditions the DAB will have different operation modes, for simplicity, the ratio of primary and secondary voltages is assumed to be similar to transformer turn ratio, i.e., $V_1 \approx nV_2$, by neglecting the influence of dead time.

Case I: $0 < D_1 \le D_2/2$

In this case, the power can only flow from the primary side to the secondary side. All switches will be turned ON at ZVS,

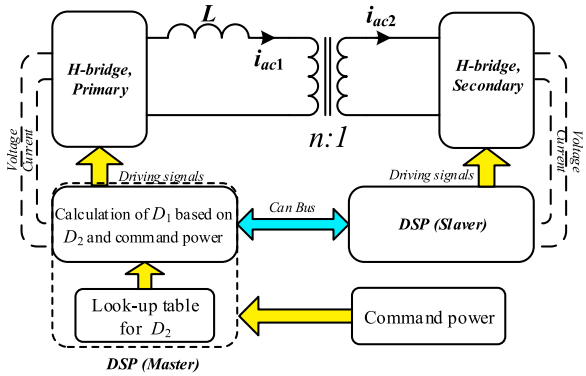

Fig. 10. Control of DBA with DPS controls.

since

$$\begin{cases} i(t_0) = \frac{((-1+D_1)V_1+(1+D_1-2D_2)nV_2)}{4Lf_s} \\ i(t_1) = \frac{((-1+D_1)V_1+(1+3D_1-2D_2)nV_2)}{4Lf_s} \\ i(t_2) = -\frac{((1+3D_1-2D_2)V_1+(-1+D_1)nV_2)}{4Lf_s} \\ i(t_3) = -\frac{((1+D_1-2D_2)V_1+(-1+D_1)nV_2)}{4Lf_s}. \end{cases} \quad (24)$$

Thus

$$\begin{cases} i(t_0) < 0, \ \ i(t_1) < 0 \\ i(t_2) > 0, \ \ i(t_3) > 0. \end{cases} \quad (25)$$

Case II: $D_2/2 < D_1 \le D_2$

In this case, the power is also transmitted from the primary side to the secondary side. From the analysis of operation modes in Section III-B, it can be summarized that S1, S2, S5, and S6 are turned ON at ZVS, while S3, S4, S7, and S8 can be switched at ZCS, i.e., one leg of H-bridge can achieve ZVS and another one can have ZCS.

Case III: $D_2 < D_1 \le (D_2 + 1)/2$

If D_1 is higher than D_2, the energy will flow from the secondary side to the primary side. The switching states are similar to those in Case II. However, in this case, S1, S2, S5, and S6 are switched at ZCS, while S3, S4, S7, and S8 are turned ON at ZVS.

Therefore, the switching losses and efficiency of using the DPS control with bidirectional inner phase shifts is similar to those of the conventional DPS control.

IV. Implementation of the DPS Control With Bidirectional Inner Phase Shifts and Verifications

A. Experimental Platform

Fig. 10 shows the platform configuration; the primary and secondary converters are controlled by two digital signal processors (DSPs) TMS320F28335 from Texas Instrument due to the flexibility. To synchronize the drive signals, two DSPs are operated in master/slave modes. Moreover, a controller area network (CAN) bus is used to connect two controllers for the data transmission. The control algorithm is implemented in the

TABLE I
CIRCUIT AND HIGH-FREQUENCY TRANSFORMER MAIN PARAMETERS

Parameters	Values
Primary dc voltage, $V_{\rm pri}$	30 V
Secondary dc voltage, $V_{\rm sec}$	30 V
Switching frequency, f_s	10 kHz
IGBT module	PS21765
Transformer turn ratio	30:30
Transformer magnetization inductance, L_m	4.3 mH
Transformer leakage inductance, L	185 μH
Primary resistance, R_p	0.075 Ω
Secondary resistance, R_s	0.075 Ω
Dead time	0.4 μs
Maximum power rating	100 W

master DSP. With the input of command power, the outer phase shift D_2 can be obtained by a lookup table. Then, the inner phase shift D_1 can be calculated by (20)–(22) from D_2 and the command power. The calculated outer and inner phase shifts ratios are sent to the slave DSP through CAN bus. No matter the conventional DPS control or the DPS control with bidirectional inner phase shifts is implemented, there is no change of the control for the secondary converter. Table I listed the main parameters of the circuit and high-frequency transformer.

Fig. 11 shows the measured voltage and current waveforms of the DAB using the DPS control with bidirectional inner phase shifts at different inner and outer phase shift ratios. By fixing D_2, it confirms that the sum of D_1 and D_2 can be higher than 1, which is not feasible for the conventional DPS control [see Fig. 11(c)]. It can also be noticed that with the increase of D_1, the current flowing through the leakage inductance will be reduced, which indicates less power transmission.

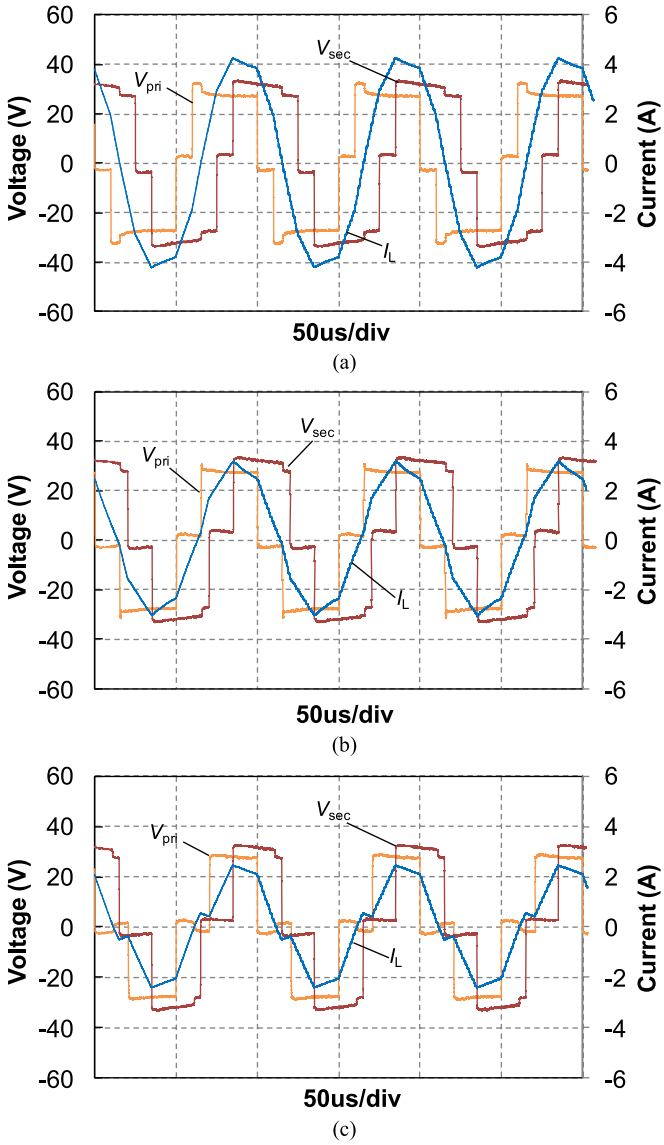

Fig. 11. Measured voltage and current waveforms in the DAB of using the DPS control with bidirectional inner phase shifts. (a) $D_1 = 0.2$, $D_2 = 0.7$. (b) $D_1 = 0.3$, $D_2 = 0.7$. (c) $D_1 = 0.4$, $D_2 = 0.7$.

B. Power Transmission Verifications

The comparisons of the measured and predicted transmission powers in the DAB of using the DPS control with bidirectional inner phase shifts are presented in Fig. 12. The transmission power against D_1 at different D_2 is shown in Fig. 12(a). Good agreements are obtained. It confirms that the maximum power transmission can be obtained at $D_1 = 0$ and $D_2 = 0.5$, which indicates that the maximum power transmission by using the DPS control with bidirectional inner phase shifts will be the same as that of using conventional DPS and SPS controls. Fig. 12(b) shows the transmission power against D_2 at different D_1. Due to the limitation of $2D_1 - D_2 \leq 1$, as D_1 increases, the feasible region of D_2 is reduced. Good agreements are obtained between the measured and predicted results.

Fig. 13 shows good agreements of reactive power comparison between the measured and predicted results. Higher reactive power can be observed at small D_1 but larger D_2 (see Fig. 13). It also confirms that if $D_1 \geq D_2/2$, zero reactive power can be obtained. Since small reactive power can help to reduce the current ripple, dc-link capacitance and further to increase the efficiency, by properly selecting the combinations of D_1 and D_2, zero reactive power and unity power factor can be achieved by using the DPS control with bidirectional inner phase shifts.

C. Control Algorithm for Constant Power Transmission

Generally, in EVs and HEVs, the battery charging with constant power is one of the commonly used strategies [21]. According to the analysis in Section III, it is shown that to implement the constant power charging, infinite D_1 and D_2 combinations can be applied. However, different combination of D_1 and D_2 will lead to different current waveforms, RMS currents, and efficiencies. Thus, in order to investigate the performance of the developed DPS control with different D_1 and D_2 combinations, D_1 is calculated by (20)–(22) with the transmission power command and D_2.

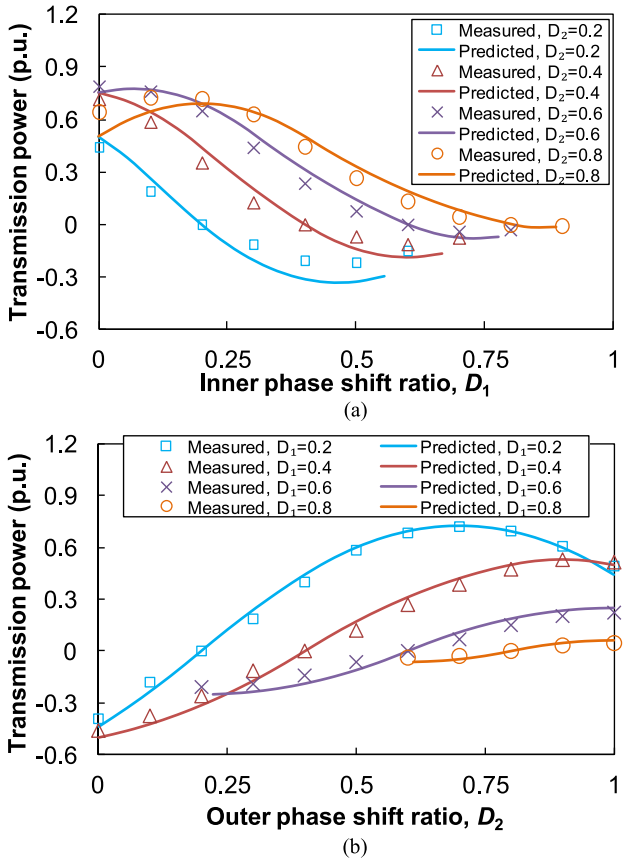

Fig. 12. Comparisons between the measured and predicted results in the DAB using the DPS control with bidirectional inner phase shifts. (a) Transmission power against D_1. (b) Transmission power against D_2.

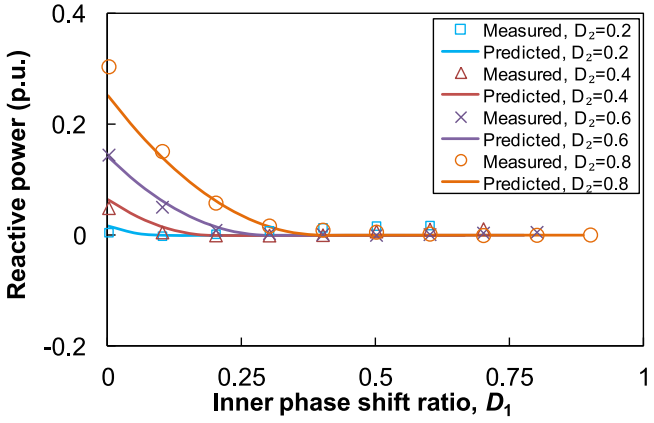

Fig. 13. Comparison of reactive power between the measured and predicted results.

Fig. 14 shows the current waveforms with different D_1 and D_2 combinations for a constant power transmission ($P/P_B = 0.4$). It is shown that the RMS currents with D_1/D_2 combination of 0/0.15, 0.27/0.47, and 0.47/0.83 are 1.11, 1.18, and 1.68 A, respectively. The difference is mainly because of different reactive powers with different D_1/D_2 combinations. Therefore, in order to obtain the optimal efficiency of the DAB, the

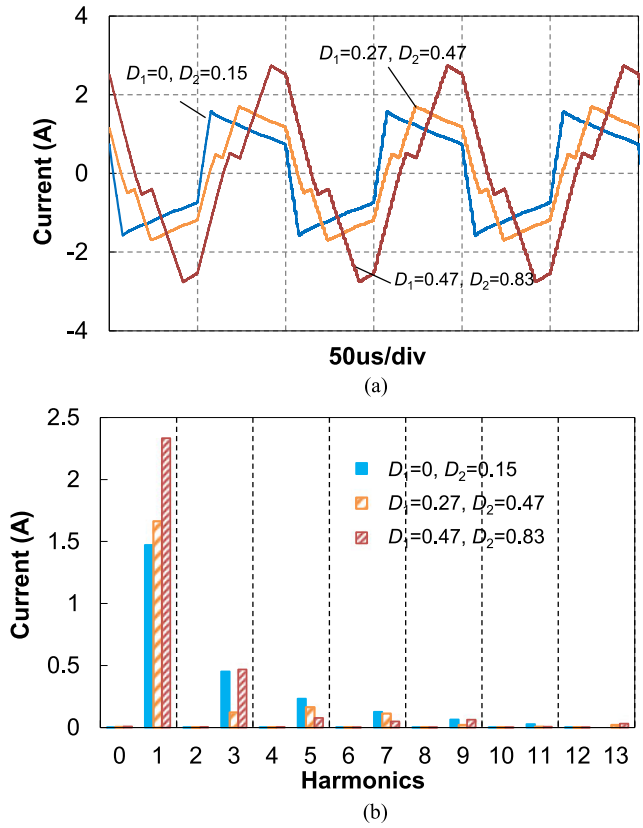

Fig. 14. Current waveforms and spectra for transmission power of $P/P_B = 0.4$ with different D_1 and D_2 combinations. (a) Current waveforms. (b) Spectra.

combination of D_1 and D_2 should be optimized, as will be presented in the next section.

V. Efficiency and Comparison With Conventional DPS

A. *Efficiency at Constant Power but Different D_1 and D_2*

Fig. 15(a) and (b) shows the measured D_1 and RMS currents in the DAB using conventional DPS and DPS controls with bidirectional inner phase shifts at transmission power (P/P_B) of 0.2, 0.4, and 0.6. It is shown that the operation region of D_2 is significantly reduced as the transmission power reduces if the conventional DPS modulation is used. However, the operation region of D_2 is almost the same regardless of the transmission power.

In addition, the test results show that as D_2 increases, higher RMS currents will be observed in both DPS controls. However, the maximum RMS currents of using the DPS control with bidirectional inner phase shifts are smaller than those of the conventional DPS control.

B. *Overall Losses and Efficiency*

Fig. 16 compares the overall losses, which are measured from the input power of primary side and output power of secondary side. Thus, the IGBT switching loss, conduction loss, transformer core loss, and copper loss are taken into account. It is

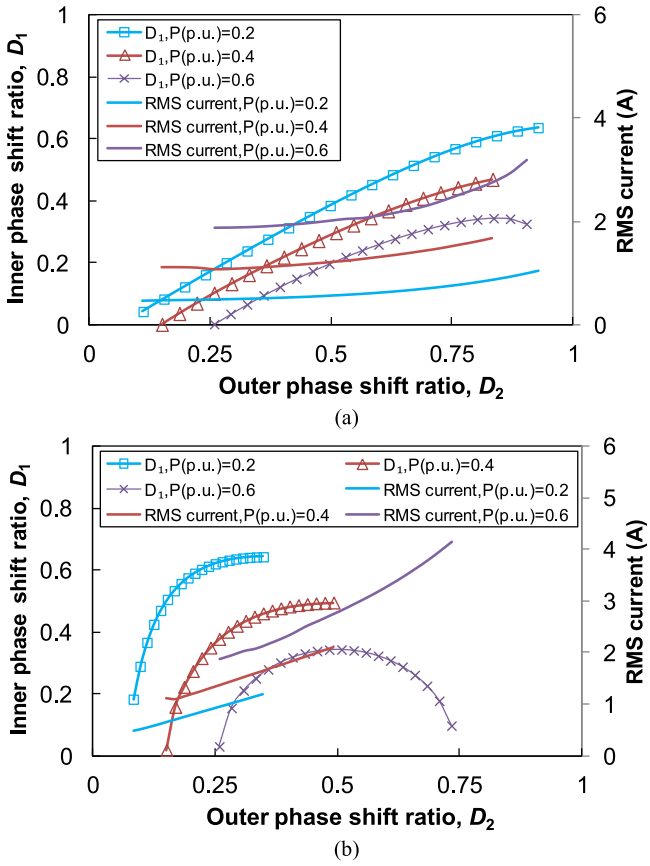

Fig. 15. Measured D_1/D_2 combinations and corresponding RMS currents using different DPS controls. (a) DPS control with bidirectional inner phase shifts. (b) Conventional DPS control.

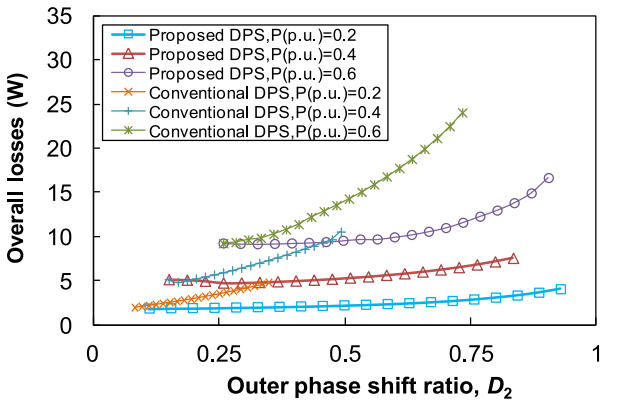

Fig. 16. Overall loss comparisons between the conventional and proposed DPS controls.

shown that the minimal overall losses of the conventional DPS control are similar to those of the DPS control with bidirectional inner phase shifts. However, the maximum losses in the conventional DPS control are much higher than those of using the proposed DPS modulation.

The measured efficiencies, which are calculated by (26), are compared in Fig. 17. It is shown that the proposed modulation can transmit the power more efficiently than the conventional

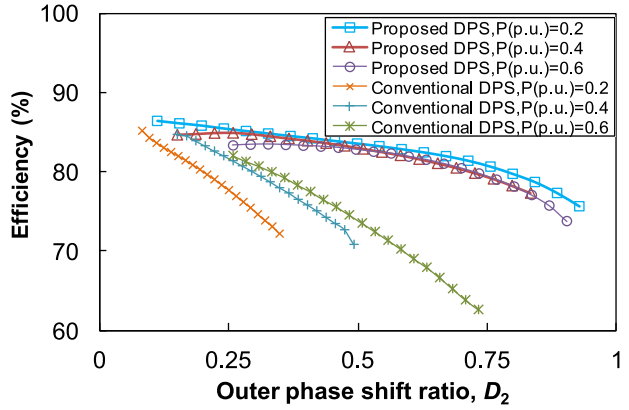

Fig. 17. Efficiency comparisons between the conventional and proposed DPS controls.

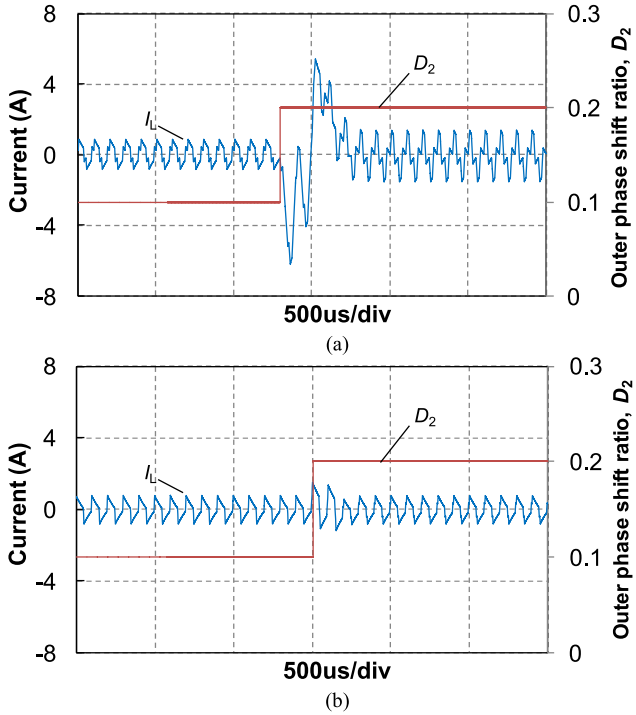

Fig. 18. Dynamic performance of current at a step change of D_2 and power transmission of 0.2 (p.u.). (a) Conventional DPS control. (b) DPS control with bidirectional inner phase shifts.

modulation

$$\eta = \frac{P_o}{P_o + P_{\text{loss}}} \times 100\%. \tag{26}$$

C. Dynamic Performance Comparisons

Fig. 18(a) and (b) compares the dynamic current waveforms at a step change of D_2 from 0.1 to 0.2 for a constant power transmission ($\mathrm{P/P_B} = 0.2$). It is shown that by using the DPS control with bidirectional inner phase shifts, much less current oscillation can be obtained. The current waveforms are more stable during the transient process. Moreover, the efficiencies

of using the DPS control with bidirectional inner phase shift are changed from 86.4% to 86.0% with the step change of D_2 from 0.1 to 0.2. However, the conventional DPS control exhibits the efficiency change from 84.3% to 78.6% during the transient process.

VI. Conclusion

In the DAB with the conventional DPS control, the inner shift directions in both the primary- and secondary-side converters are the same. Hence, the sum of inner and outer phase shift ratio is required to be less than 1, i.e., $D_1+\mathrm{D}_2\leq 1$, which results in the narrow operation region of D_2 particularly at light load. Therefore, significant variations of D_1 cannot be avoided if there is a small disturbance of D_2, which will result in high surge current and low stability of the system, particularly at light load.

To solve this problem, a novel DPS control with bidirectional inner phase shifts is proposed in this paper. Based on the analysis of operation modes and power characteristic of using DPS with bidirectional inner phase shifts, the operation regions of D_1 and D_2 can be significantly enlarged particularly at light load, as also confirmed by the test results. Moreover, from the experimental verification, it is shown that compared with the conventional DPS modulation, the surge current can be significantly reduced with the variation of D_2. High stability of the DAB with the proposed method can be obtained without scarifying the efficiency particularly at light load. With the verifications, it should be mentioned that the voltage is not restricted to 30 V. Higher voltage and power can also be applied and its verification will be the future work. In addition, a bidirectional power flow can be achieved with D_1 and D_2 operation region of 0–1.

References

[1] R. De Doncker, D. M. Divan, and M. H. Kheraluwala, "A three phase soft-switched high-power-density dc/dc converter for high-power applications," *IEEE Trans. Ind. Appl.*, vol. 27, no. 1, pp. 63–73, Jan./Feb. 1991.

[2] J. Walter, and R. De Doncker, "High-power galvanically isolated dc/dc converter topology for future automobiles," in *Proc. 34th IEEE Power Electron. Spec. Conf.*, Jun. 2003, pp. 27–32.

[3] H. J. Chiu and L. W. Lin, "A bidirectional DC–DC converter for fuel cell electric vehicle driving system," *IEEE Trans. Power Electron.*, vol. 21, no. 4, pp. 950–958, Jul. 2006.

[4] S. Inoue, and H. Akagi, "A bidirectional dc-dc converter for an energy storage system with galvanic isolation," *IEEE Trans. Power Electron.*, vol. 22, no. 6, pp. 2299–2306, Nov. 2007.

[5] Y. Xie, J. Sun, and J. S. Freudenberg, "Power flow characterization of a bidirectional galvanically isolated high-power dc/dc converter over a wide operating range," *IEEE Trans. Power Electron.*, vol. 25, no. 1, pp. 54–66, Jan. 2010.

[6] H. Akagi, T. Yamagishi, N. M. L. Tan, S. Kinouchi, Y. Miyazaki, and M. Koyama, "Power-loss breakdown of a 750V 100kW 20kHz bidirectional isolated dc-dc converter using SiC-Mosfet/SBD dual modules," *IEEE Trans. Power Electron.*, vol. 51, no. 1, pp. 420–428, Jan./Feb. 2015.

[7] G. Oggier, and M. Ordonez, "High efficiency DAB converter using switching sequences and burst-mode," *IEEE Trans. Power Electron.*, vol. 31, no. 3, pp. 2069–2082, Mar. 2016.

[8] J. Hiltunen, V. Vaisanen, R. Juntunen, and P. Silventoinen, "Variable-frequency phase shift modulation of a dual active bridge converter," *IEEE Trans. Power Electron.*, vol. 30, no. 12, pp. 7138–7148, Dec. 2015.

[9] Y. Wang, S. W. H. de Haan, and J. A. Ferreira, "Optimal operating ranges of three modulation methods in dual active bridge converters," in *Proc. IEEE 6th Int. Power Electron. Motion Control Conf.*, Wuhan, China, May 17–20, 2009, pp. 1397–1401.

[10] F. Krismer and J. W. Kolar, "Closed form solution for minimum conduction loss modulation of DAB converters," *IEEE Trans. Power Electron.*, vol. 27, no. 1, pp. 174–188, Jan. 2012.

[11] A. Jain and R. Ayyanar, "PWM control of dual active bridge: Comprehensive analysis and experimental verification," *IEEE Trans. Power Electron.*, vol. 26, no. 4, pp. 1215–1227, Apr. 2011.

[12] H. Tao, A. Kotsopoulos, J. L. Duarte, and M .A. Hendrix, "Transformer-coupled multiport ZVS bidirectional dc-dc converter with wide input range," *IEEE Trans. Power Electron.*, vol. 23, no. 2, pp. 771–781, Mar. 2008.

[13] G. G. Oggier, R. Ledhold, G. O. Garcia, A. R. Oliva, J. C. Balda, and F. Barlow, "Extending the ZVS operating range of dual active bridge high-power dc-dc converters," in *Proc. 37th IEEE Power Electron. Spec. Conf.*, Jeju, South Korea, Jun. 2006, pp. 1–7.

[14] G. G. Oggier, G. O. Garcia, and A. R. Oliva, "Switching control strategy to minimize dual active bridge converter losses," *IEEE Trans. Power Electron.*, vol. 24, no. 7, pp. 1826–1836, Jul. 2009.

[15] G. G. Oggier, G. O. Garcia, and A. R. Oliva, "Modulation strategy to operate the dual active bridge dc-dc converter under soft switching in the whole operating range," *IEEE Trans. Power Electron.*, vol. 26, no. 4, pp. 1228–1236, Apr. 2011.

[16] F. Krismer, S. Round, and J. Kolar, "Performance optimization of a high current dual active bridge with a wide operating voltage range," in *Proc. 37th IEEE Power Electron. Spec. Conf.*, Jeju, South Korea, Jun. 2006, pp. 1–7.

[17] H. Zhou, and A. M. Khambadkone, "Hybrid modulation for dual-active-bridge bidirectional converter with extended power range for ultracapacitor application," *IEEE Trans. Ind. Appl.*, vol. 45, no. 4, pp. 1434–1442, Jul./Aug. 2009.

[18] F. Krismer, and J. Kolar, "Efficiency-optimized high-current dual active bridge converter for automotive applications," *IEEE Trans. Ind. Electron.*, vol. 59, no. 7, pp. 2745–2760, Jul. 2012.

[19] H. Bai, and C. Mi, "Eliminate reactive power and increase system efficiency of isolated bidirectional dual-active-bridge DC-DC converter using novel dual-phase-shift control," *IEEE Trans. Power Electron.*, vol. 23, no. 6, pp. 2905–2914, Nov. 2008.

[20] B. Zhao, Q. Song, and W. Liu, "Power characterization of isolated bidirectional dual-active-bridge DC-DC converter with dual-phase-shift control," *IEEE Trans. Power Electron.*, vol. 27, no. 9, pp. 4172–4176, Sep. 2012.

[21] Y. Wang, Y. Wu, and T. Lee, "Design and implementation of a bidirectional isolated dual-active-bridge-based dc/dc converter with dual-phase –shift control for electric vehicle battery," in *Proc. Energy Convers. Congr. Expo.*, Sep. 2013, pp. 5468–5475.

[22] K. Wu, C. W. de Silva, and W. G. Dunford, "Stability analysis of isolated bidirectional dual active full-bridge dc-dc converter with triple phase-shift control," *IEEE Trans. Power Electron.*, vol. 27, no. 4, pp. 2007–2017, Apr. 2012.

[23] B. Zhao, Q. Song, and W. Liu, "Efficiency characterization and optimization of isolated dc-dc converter based on dual-phase-shift control for dc distribution application," *IEEE Trans. Power Electron.*, vol. 28, no. 4, pp. 1711–1727, Apr. 2013.

[24] S. P. Engel, N. Soltau, H. Stagge, and R. W. Doncker, "Dynamic and balanced control of three-phase high-power dual-active bridge dc-dc converters in dc-grid applications," *IEEE Trans. Power Electron.*, vol. 28, no. 4, pp. 1880–1889, Apr. 2013.

X. Liu (M'13–SM'16) received the B.Eng. and Ph.D. degrees in electrical engineering from Zhejiang University, Hangzhou, China, in 2005 and 2010, respectively.

In 2010, he joined the Department of Electronics and Electrical Engineering, The University of Sheffield, Sheffield, U.K., where he was a Research Associate from 2012 to 2015. In 2015, he was a Software Development Engineer with Controlled Power Technologies Ltd. He is currently a Professor with Hebei University of Technology, Tianjin, China. His research interests include design and application of switched reluctance machines, permanent magnet machines, and dc/dc converters.

Z. Q. Zhu (M'90–SM'00–F'09) received the B.Eng. and M.Sc. degrees in electrical and electronic engineering from Zhejiang University, Hangzhou, China, in 1982 and 1984, respectively, and the Ph.D. degree in electrical and electronic engineering from the University of Sheffield, Sheffield, U.K., in 1991.

He joined the University of Sheffield in 1988, where he has been a Professor of electrical machines and control systems since 2000 and is currently the Head of the Electrical Machines and Drives Research Group and the Royal Academy of Engineering/Siemens Research Chair. His current major research interests include design and control of permanent-magnet brushless machines and drives for applications ranging from automotive and aerospace to renewable energy.

David A. Stone received the B.Eng. degree in electronic engineering from the University of Sheffield, Sheffield, U.K., in 1984, and the Ph.D. degree from Liverpool University, Liverpool, U.K., in 1989.

He is currently a Professor of electrical engineering with the University of Sheffield, where he has been since 1989, joining the Electrical Machines and Drives group as a member of academic staff responsible for power electronics and energy storage.

Martin P. Foster received the B.Eng. degree in electronic and electrical engineering, the M.Sc.(Eng.) degree in control systems, and the Ph.D. degree for his thesis "Analysis and Design of High-order Resonant Power Converters" all the University of Sheffield, Sheffield, U.K., in 1998, 2000, and 2003, respectively.

Since 2003, he has been a member of the academic staff in the Department of Electronic and Electrical Engineering, The University of Sheffield, where he is involved in power electronic systems. His current research interests include the modeling and control of switching power converters, resonant power supplies, multilevel converters, battery management, piezoelectric transformers, power electronic packaging, and autonomous aerospace vehicles.

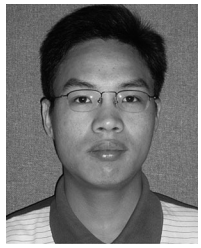

W. Q. Chu received the B.Eng. degree from Zhejiang University, Hangzhou, China, and the M.Sc. degree from Huazhong University of Science and Technology, Wuhan, China, in 2004 and 2007, respectively, both in electrical engineering, and the Ph.D. degree in the electronic and electrical engineering from the University of Sheffield, Sheffield, U.K., in 2013.

From 2007 to 2009, he was with Delta Electronics (Shanghai) Co., Ltd. From 2012 to 2014, he was a Postdoctoral Research Associate with the University of Sheffield, where he is currently a Principal Design Engineer at Sheffield-CRRC Electric Drives Technology Research Centre. His major research interests include the design and analysis of novel machines for wind power and electric vehicle applications.

Iain Urquhart received the B.Sc. (Hons.) degree in artificial intelligence and robotics from Robert Gordon University, Aberdeen, U.K., in 2004. He is currently working toward the Ph.D. degree in electric machines with the University of Sheffield, Sheffield, U.K.

He joined the Nissan Graduate scheme in 2004 and worked in Chassis mechatronics design for six years, responsible for ABS/ESP, EPAS, and TPMS on B and C platform vehicles for the European market. He joined the Nissan Europe Advanced Engineering group in 2009 and was seconded to the University of Sheffield in 2010 as an Embedded Engineer managing joint research projects on EV electric powertrains and drives. In early 2016, he went on sabbatical from Nissan to study for his Ph.D. research.

James Greenough was born in the U.K. in 1977. He received the B.Eng. degree from Manchester Metropolitan University, Manchester, U.K., in 1999, and the M.Sc. degree in advanced control and systems engineering from the University of Manchester, Manchester, in 2008.

His main research interests include power electronics, high-precision switching techniques, and future powertrain development.